Chinese Chemical Letters 37 (2026) 111960

Contents lists available at ScienceDirect

Chinese Chemical Letters

journal homepage: www.elsevier.com/locate/cclet

Current advances in heterogeneous catalysts based on hypercrosslinked polymers for transesterification in biodiesel production: A comprehensive review

Yuheng Wen[a], Zeyu Wang[a], Jingli Li[a], Chengyao Xue[a], Haobo Wang[a], Xingrui Li[a], Hao Zhang[a], Yang Lu[b], Yu Zhang[c,*], Qing Hou[d,*], Wenliang Song[a,*]

[a] School of Materials and Chemistry, University of Shanghai for Science and Technology, Shanghai 200093, China
[b] Fuzhou LBE Pharma Tech. Co., Ltd., Fuzhou 350000, China
[c] School of Pharmacy, Shanghai University of Medicine & Health Sciences, Shanghai 201318, China
[d] School of Artificial Intelligence Science and Technology, University of Shanghai for Science and Technology, Shanghai 200093, China

ARTICLE INFO

Article history:
Received 21 July 2025
Revised 11 October 2025
Accepted 13 October 2025
Available online 15 October 2025

Keywords:
Hypercrosslinked polymers
Green synthesis
Catalyst design
Highly accessible active site
Biodiesel production

ABSTRACT

The growing global demand for sustainable energy makes biodiesel an important renewable alternative to alleviate the energy crisis and reduce greenhouse gas emissions. Therefore, there is an urgent need to develop efficient, environmentally friendly and economically viable biodiesel production methods. Hypercrosslinked polymers (HCPs), as aromatic porous organic polymers, are solid frameworks that can be used as heterogeneous catalyst, and they are a promising platform for biodiesel catalytic conversion due to their low cost, highly accessible active site, tunable catalytic site types. In addition, innovative green synthesis strategies make environmentally begin production of HCPs possible. In recent years, HCPs has developed rapidly in the field of biomass catalysis. Unfortunately, to the best of our knowledge, there are no publications focusing on the green synthesis and application of HCPs-based materials for biodiesel production. This review provides an update on the synthesis and utilisation of green and efficient HCPs for catalytic biodiesel production. Initially, the green routes for HCPs synthesis are described, followed by a comprehensive summary of the various approaches to biodiesel production. The primary focus is on the utilisation of HCPs as carriers of active sites in the catalytic conversion of biodiesel, with particular emphasis on catalyst design, morphology control, and intelligent management in terms of application extension. Ultimately, thought-provoking recommendations are proposed to utilize improved green HCPs in combination with advanced production processes to achieve more efficient and sustainable development.
© 2026 Published by Elsevier B.V. on behalf of Chinese Chemical Society and Institute of Materia Medica, Chinese Academy of Medical Sciences.

1. Introduction

As a major source of fossil fuel consumption and greenhouse gas emissions, the transport industry is under increasing pressure to adapt to the global climate crisis and the shift toward sustainable energy [1–5]. According to the International Energy Agency, the demand for liquid biofuels in 2024 is 0.2 EJ higher than in previous years, accounting for more than 4% of global transport fuel consumption [6]. This also reflects higher biofuel blending requirements and fuel consumption in the context of continued policy support and growing transport fuel demand [7,8]. It is worth noting that in this wave of green transformation, biodiesel is becoming one of the most promising alternatives to fossil fuel diesel by virtue of its low carbon emissions, renewable raw materials and compatibility with the existing diesel infrastructure [9–11]. Biodiesel is considered a more environmentally friendly option compared to conventional diesel because it produces fewer harmful emissions, such as carbon monoxide, particulate matter, and sulfur oxides. Additionally, because it is derived from renewable resources, biodiesel helps reduce dependence on fossil fuels and lowers the overall carbon footprint [12,13]. Biodiesel can be used in pure form (B100) [14] or blended with petroleum diesel in various concentrations [15], such as B20 (20% biodiesel and 80% petroleum diesel) [16,17]. The use of biodiesel benefits agricultural industries, reduces greenhouse gas emissions, and contributes to a more sustainable energy future. This process involves reacting oils or fats with an alcohol (usually methanol) and a catalyst (typically an acid or base) to produce biodiesel fatty acid methyl ester (FAME) and

* Corresponding authors.
E-mail addresses: zhangy_21@sumhs.edu.cn (Y. Zhang), qinghou@usst.edu.cn (Q. Hou), wenliang@usst.edu.cn (W. Song).

https://doi.org/10.1016/j.cclet.2025.111960
1001-8417/© 2026 Published by Elsevier B.V. on behalf of Chinese Chemical Society and Institute of Materia Medica, Chinese Academy of Medical Sciences.

glycerol as a byproduct [18–21]. Commonly, biodiesel is produced from vegetable oils, animal fats, or recycled cooking oil through transesterification. Thus, the catalysts often play important role in biodiesel production.

Acid catalysis plays a crucial role in numerous industrial chemical processes and is extensively utilized across various sectors, including petroleum refining [22], water and gas purification [23], organic synthesis [24] and biomass conversion [25,26]. Homogeneous acid catalysts, such as sulfuric acid (H_2SO_4), phosphoric acid, and trifluoromethanesulfonic acid, are commonly used in these processes due to their affordability and excellent catalytic efficiency [27–29]. However, these mineral acids are not reusable and contribute to significant corrosion, waste, and environmental issues. As a result, extensive research has focused on developing solid acid catalysts that can be recycled [30,31]. Materials like metals [32,33], metal oxides [34,35] and non-metallic substances with acidic group [36] are promising alternatives, as they are easy to store and transport, offering a safer and more environmentally sustainable option. Additionally, these materials can be easily separated and reused multiple times.

Nanoporous organic polymers (NOPs) are the class of polymer frameworks that only consisting of the lighter elements such as C, H, O, N [37–40]. Hypercrosslinked polymers (HCPs) are one kind of NOPs with the designable cross-linked rigid structures, hierarchal amorphous pore size distributions, and controllable external morphologies [41,42]. HCPs can be synthesized through simple and safe methods, without the requirement for expensive catalysts, inert atmospheres, or complex monomers. Owing to their low cost, highly accessible active sites, tunable catalytic functionalities, and ease of recovery, HCPs represent a highly promising platform for advancing biodiesel production processes [43,44]. In recent years, HCPs have gained prominence as heterogeneous catalyst supports, exhibiting exceptional potential in biodiesel synthesis by enabling the incorporation of acid, base, and enzymatic active sites onto their surfaces. Their well-controlled porosity further mitigates the leaching of active species into biodiesel products. Additionally, the inherent synthetic versatility of HCPs facilitates morphological engineering (*e.g.*, hollow spheres, nanofibers) [45–47] to enhance the accessibility of active sites. By integrating green synthetic strategies, such as metal-free catalysis and solvent-free mechanochemistry [48], with artificial intelligence [49,50], HCP-based catalysts have increasingly aligned with sustainable paradigms for biodiesel production, addressing both energy and environmental challenges. Furthermore, the mechanical robustness and solvent resistance of HCPs support their application in continuous-flow reactors, thereby enabling scalable and efficient biodiesel production.

To date, although a limited number of review articles have been published in related fields, they have primarily concentrated on biodiesel production itself. Notably, to the best of our knowledge, no comprehensive reviews have addressed the green synthesis and application of HCPs-based materials specifically for biodiesel production. This review aims to fill that gap by providing an updated overview of the synthesis and utilization of improved, green, and efficient HCPs for catalytic biodiesel production (Fig. 1). It begins by highlighting the significance of biodiesel as a sustainable alternative fuel and discussing the limitations of conventional catalysts, thereby motivating the need for greener synthetic routes for HCPs. Subsequently, the intrinsic properties of HCPs that influence their catalytic performance are explored, followed by a thorough analysis of the various methodologies and factors impacting biodiesel production. Particular attention is given to the use of HCPs as carriers for active catalytic sites, with a focus on their swelling behavior, porosity, and sulfur content. Remarkably, the intelligent management during the biodiesel production is also highlighted. Finally, the review proposes constructive strategies for the development of enhanced green HCPs, integrated with advanced production technologies, to achieve more efficient and sustainable biodiesel production.

2. Green approaches of HCPs

Initially found by Davankov in 1970 [51,52], the typical synthetization method was utilized a benzyl chloride contained polystyrene as the precursor. After it swollen in the 1,2-dichloroethane and followed knitting *via* classical Friedel-crafts reaction by the Lewis acid catalysts such as $FeCl_3$, the methylene linked aromatic rings of polystyrene were highly crosslinked, that is the reason why so called as HCPs. Attributed with these properties by synthetization, the direct application is relevantly with gas capture and solvent storage. The CO_2, hydrogen, and methane are all reported as the represented model for absorption and showing comparable absorption ability as other microporous polymers [53,54]. With the development of HCPs synthesizing, three methods: (1) The one-step polycondensation, (2) post-crosslinking of polymers, and (3) external crosslinking of the aromatic monomers, have become the mainstream to generate the diverse HCPs materials. Meanwhile, the interesting functions and enhanced performances also came into being by the designable tunable structures, special functionalities, and well-defined morphologies of new discovered HCPs. To date, HCPs have been reported in pollutants removal [55], separation [56], catalysis [57], drug delivery [58], sensors [59], antibacterial materials [60], carbon precursors [61] and many other fields [62].

However, the practical and sustainable development of HCPs remains hindered by several synthetic challenges [63,64], including the reliance on metal-based Lewis acid catalysts that generate harmful by-products, as well as limitations in monomer and crosslinker design, morphology control methods, and catalyst selection. Indeed, to make HCPs become a practical utilizable material, these obstacles must be jumped for enabling a wide range of sustainable applications.

To address these synthetic challenges in a comprehensive manner, detailed explorations of four critical dimensions: crosslinker design, monomer optimization, catalysts optimization, and morphology control, are systematically presented in Texts S2.1-S2.4 (Supporting information), enabling a holistic analysis of sustainable fabrication of HCPs strategies while maintaining textual conciseness.

3. Intrinsic properties guiding catalytic behavior

3.1. Swellability

The swelling behavior of HCPs is one of the key parameters for evaluating its performance [65–67]. Unlike rigid inorganic carriers, HCPs exhibit a highly crosslinked yet inherently flexible framework. Although HCPs cannot be dissolved in common solvents, the relatively large organic molecules of solvents can penetrate into the polymer interior and interact sufficiently with the polymer chains, thereby occupying the voids within the network and causing the originally compact structure to expand [68,69]. The swelling behavior of HCPs is influenced by various parameters, including the type of initial monomers [70], polymer chain length [71], polymer polarity [72–74], crosslinking density and the solvation state of the growing polymer chains [75–78]. Excellent swelling capacity endows the polymer chains with superior flexibility, which facilitates the approach of reactants to catalytic sites.

Achieving controlled synthesis of nanoporous polymers with tailored morphologies remains a key challenge for optimizing their performance in applications that demand rapid molecular transport and accessibility, while preserving their unique

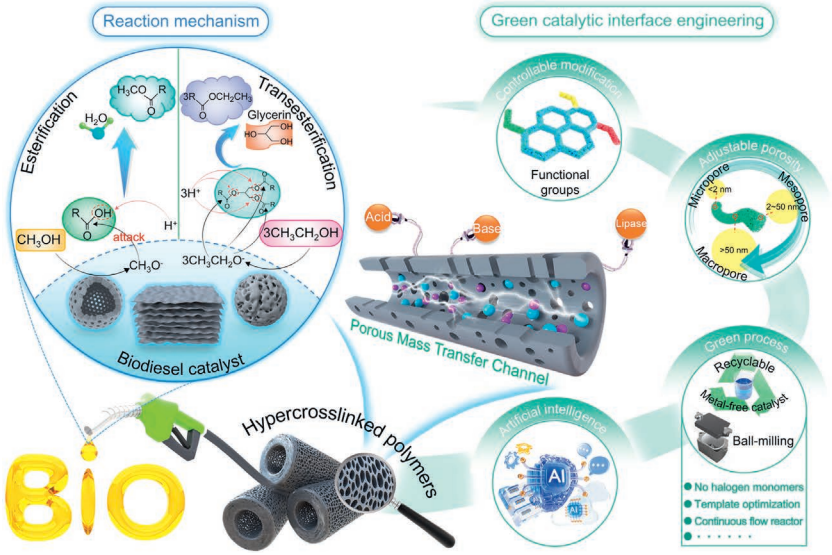


Fig. 1. Reaction mechanism of biodiesel catalysts based on HCPs and green catalytic interface engineering.

swellability [58,79,80]. Our groups systematically compared a series of morphology-controlled HCPs for their swelling behavior in methanol, dimethylformamide (DMF), and DCM [81]. Despite their high cross-linking densities, all samples exhibited significant solvent-induced swelling, with the dimensions of both micropores and mesopores enlarged in the swollen state, which may significantly enhance molecular diffusion in applications such as catalysis and adsorption. Notably, the hairy-shelled HHNP B exhibited the highest swelling capacity (~45 mL/g) in DMF (Fig. 2a), outperforming other structures and commercially available Merrifield resins. Moreover, even the HNTs, which had the lowest BET surface area, demonstrated superior swelling performance compared to the other structures, indicating that swelling capacity is not solely determined by surface area but arises from the synergistic effects of multiple factors. The authors also proposed that the swelling of HCP is largely independent of the nature of the solvent or the guest molecule, which was subsequently confirmed in swelling tests in three chemical warfare agent (CWA) simulants. In the final solubility test with real CWA (Fig. 2b), toluene- and fluorobenzene-derived HCPs exhibited a significant uptake of ~20 mL/g, Hill *et al*. embedded an oxidation system composed of tribromide, nitrate, and acid ($NO_xBr_xH^+$) into a fluorobenzene HCPs, a methylated HCP, and an HCP with acidic moieties (HCP-A) [82]. Although all three systems performed well in capturing and converting the CWA simulant, the built-in Brønsted acidic functional groups in HCP-A more effectively promoted the catalytic oxidation reaction, which eliminated the need for an exogenous acid and streamlined the overall system (Fig. 2c). Moreover, HCP-A exhibited excellent swelling behaviour in dimethyl sulfoxide (~16.2 mL/g), thereby enhancing the chelation of the simulant and facilitating intimate contact between the encapsulated species and the catalytic system. Altogether, such progress strongly promotes the evolution of multifunctional catalytic decontamination materials. Catalytic conversion of CO_2 to value-added cyclic carbonates remains a key strategy for carbon utilisation and one of the major hotspots [83–85]. Wen and coworkers proposed an innovative amide-functionalized hypercrosslinked cationic polymer, P(MBA-V_3Br)-2 [86]. Although the strong electrostatic interactions among the imidazole units prevented solvent molecules from penetrating the polymer network, the incorporation of amide groups as hydrogen-bond donors weakened these interactions. This modification increased the polymer's swelling ability toward epoxide substrates (Fig. 2d), which enhanced the exposure of active sites and accelerated the mass transfer of reactants within the network [87,88]. This excellent swelling ability also stems from the increased amide content and lower degree of crosslinking.

Under specific polymer structure design and functional group introduction conditions, the type and polarity of the solvent may still have a modulating effect on the microstructure and degree of swelling of HCPs [89]. Huang *et al*. designed an efficient yolk–shell nano-reactor that was capable of encapsulating various ligand-free metal nanoparticles within its cavity, thereby facilitating the tuning of their catalytic functionalities [90]. The most prominent highlight was the ability to regulate the free volume of the nanosphere shell by adjusting the solvent polarity that governed its swelling behavior, which in turn enabled the fine-tuning of the bimodal micropore dimensions. Upon solvent removal, the shell recovered its original state, indicating that such solvent-dependent swelling behavior was reversible (Fig. 2e).

Polymerisation induced microphase separation (PIMS) is a strategy to develop nanostructured materials with highly tunable structural domain sizes and morphologies by driving microphase separation of block copolymers during polymerisation [91]. Seo's groups first explored the formation of hierarchically porous polymers through the hypercrosslinking of PIMS monomers in 2014 [92]. In this process, an appropriate solvent was used to swell the entire PIMS, after the hypercrosslinking process, the polylactide domains were etched, and the swollen network structure produced a large number of micropores (Fig. 2f). However, for certain applications, excellent swelling performance does not confer benefits and may even be counterproductive [93–95]. Yi *et al*. developed HCP isoporous block copolymer membranes that, when subjected to prolonged immersion in solvents of varying polarity, exhibited rigid pore characteristics and highly stable pore architectures that underwent minimal swelling (Fig. 2g) [96], thereby offering extraordinary potential for the precise and on-demand separation of high-value nanoparticles with target sizes in organic solvents.

From a catalytic science perspective, the core link between swellability and catalytic behavior lies in how the dynamic framework expansion optimizes mass transfer and enhances the accessibility of active sites. In biodiesel production, this "pore breathing" effect markedly increases the diffusion rate and penetration depth of reactants toward the catalytic sites. Moreover, the

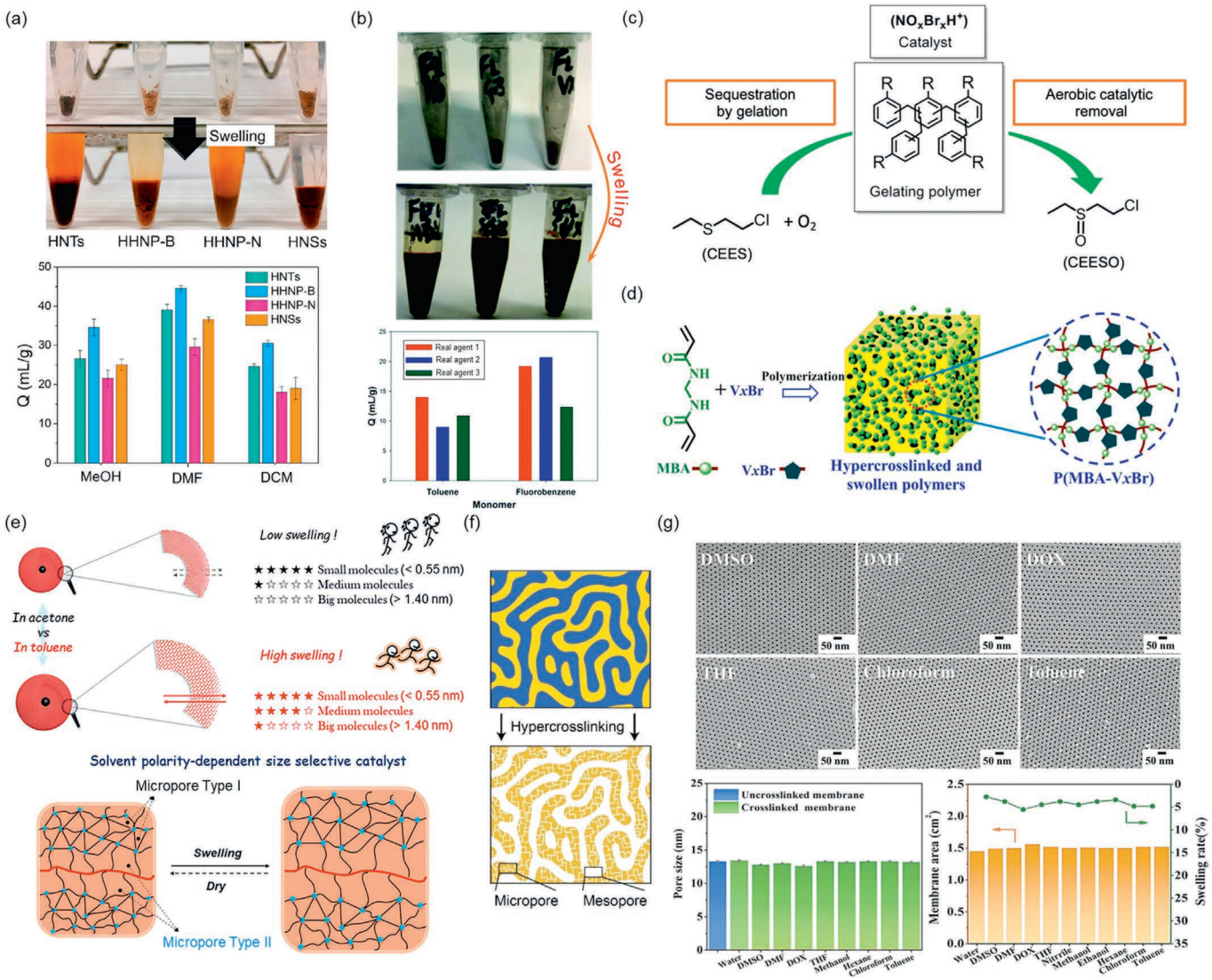


Fig. 2. (a) Optical photographs of diverse morphology-controlled HCPs before and after MeOH swelling and evaluation of swelling capacity under three different solvents. Copied with permission [81]. Copyright 2019, American Chemical Society. (b) Before and after swelling of CWA by fluorobenzene-derived HCPs and swellability of toluene- and fluorobenzene-derived HCPs for three CWAs. Reproduced with permission [70]. Copyright 2017, The Royal Society of Chemistry. (c) Aerobic catalytic removal of the sulfur mustard simulant is achieved *via* the catalytic oxidation system embedded within the gelating polymer. Copied with permission [82]. Copyright 2021, American Chemical Society. (d) Schematic representation for preparing crosslinked and swollen polymers. Copied with permission [86]. Copyright 2022, Elsevier Publishing Group. (e) Solvent polarity-dependent size-selective catalysts have better swelling and richer pores in toluene and the swelling behavior is reversible. Copied with permission [90]. Copyright 2019, American Chemical Society. (f) Simultaneous hypercrosslinking and etching of a PIMS precursor to create a hierarchical meso– and micro-porous material. Copied with permission [91]. Copyright 2023, Wiley Publishing Group. (g) SEM images of surface morphology after two months of immersion in different organic solvents, as well as pore size changes and swelling ratio evaluation. Copied with permission [96]. Copyright 2024, Wiley Publishing Group.

chain flexibility introduced by swelling facilitates a higher contact frequency and affinity between functional groups and substrates.

3.2. Porosity

Since the 1970s, hypercrosslinking, generally of polymers containing aromatic groups in a swollen state of solvent by Friedel-Crafts alkylation [42,71,97–99], has produced new cross-links, thus introducing a large number of micropores in the network phase, which are able to maintain a high level of micro-porosity even after removal of the solvent. It has been widely acknowledged that incorporation of mesopores in microporous materials to form layered structures is a promising way to remove their transport limitations and further enhance their value in catalytic applications [100–104]. By integrating the high specific surface area provided by micropores and the rapid mass transfer pathways to the internal surfaces enabled by mesopores, further introduction of macropores can effectively minimize diffusion distances, thereby establishing a more optimized structural foundation for efficient catalysis [105–108].

In the report by the Silverstein group, a one-pot method was innovatively applied to combine two polymer systems to construct simultaneous interpenetrating polymer networks (IPN) [109]. Notably, the IPN based on 1,6-diisocyanatohexane (HDI), termed IPN–H, produced mesopores with a median pore width of 6.7 nm following hypercrosslinking, the generation of mesoporosity reflected the $FeCl_3$-catalyzed degradation of these larger phase separated domains in IPN–H during hypercrosslinking, thereby significantly enhancing the hierarchical porous structure (Fig. 3a). Compared to strategies for constructing static pore structures, the dynamic modulation of porosity *via* the swelling characteristics of HCPs is equally compelling. In the core–shell nanoreactor devel-

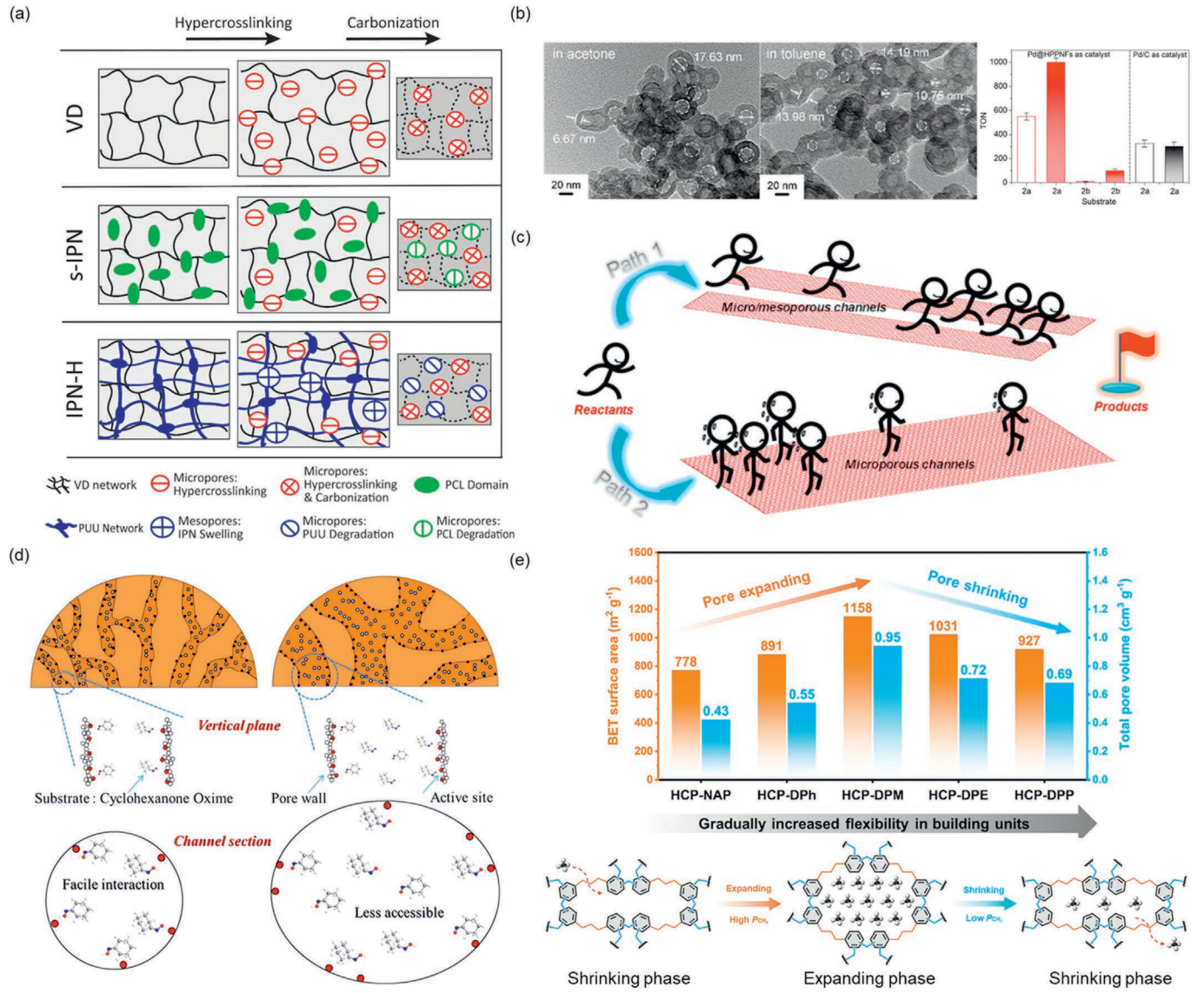


Fig. 3. (a) Schematic illustrations of micropore and mesopore generation: without porogenic agent (VD), semi-IPN containing PCL-triol, IPN containing HDI-based poly(urethane urea) network. Copied with permission [109]. Copyright 2022, American Chemical Society. (b) Representative TEM images of egg yolk shell nanoreactors immersed in toluene and acetone and hydrogenation of alkene-modified calixarenes by nanoreactors. Hollow and filled columns represent acetone and toluene, respectively. Copied with permission [90]. Copyright 2019, American Chemical Society. (c) Introduction of mesoporous channels in micropores enables faster product leave in the reduction pathway. Copied with permission [110]. Copyright 2017, Elsevier Publishing Group. (d) Schematic illustration of how pore structure affects catalytic efficiency. Copied with permission [44]. Copyright 2015, Elsevier Publishing Group. (e) The impact of building unit flexibility on total pore volumes and BET surface areas. Reproduced with permission [111]. Copyright 2025, Wiley Publishing Group.

oped by Huang *et al.*, the shell swelled to approximately 14.0 nm in nonpolar toluene, twice the thickness observed in weakly polar acetone (~6.6 nm), and this change in shell thickness consequently altered the polymer surface's type-I micropores (~0.55 nm) and type-II micropores (~1.40 nm) (Fig. 3b) [90]. In Pd nanoparticle-encapsulated nanoreactors, subsequent hydrogenation reactions of two alkene-modified calixarenes revealed that the turnover numbers in a toluene environment exceeded those in acetone, a result attributed to the swelling-induced increase in micropore size. As shown in Fig. 3c, Huang's group further confirmed that the mesoporous channels play a key role in the reactant as the catalyst for accelerating the speed of reaction. In which the mesopore could help the reactant flow effectively during the reaction [110]. The confined pore size is benefit for the special catalysis applications. As depicted in Fig. 3d, Wang's group showed the sulfonic acid functionlized HCPs could adjusted by monomer selection and sulfonation degree, after carefully selection, the resulted catalysts not only exhibited the high sulfonation (2.41 mmol/g) with the high surface area (>1000 m^2/g), but also showed the special nano-confinement effect with the special narrow pore size distribution at the junction region of micro, and mesopore size (~2 nm) [44]. As shown in Fig. 3e, Tan *et al.* employed an external crosslinking strategy to adjust the aliphatic chain length within biphenyl structural units, thereby systematically controlling the flexibility of the resulting HCPs frameworks [111]. Under specific methane pressures, these flexible polymers exhibited pore Notably, the HCP based on 1,3-diphenylpropane displayed a higher packing density (0.68 g/cm^3) and, by incorporating a longer propylene bridging chain (-CH_2-CH_2-CH_2-), manifested a unique gate-opening effect that enabled an exceptional volumetric methane uptake of 333 cm^3 STP cm^{-3} at 273 K and 100 bar. This finding has marked a significant step toward the development of economically efficient, high-capacity flexible porous adsorbents for practical methane storage applications.

From a catalytic science perspective, this network of interconnected pores not only provides abundant surface-active sites, but also forms continuous molecular channels, significantly reducing macroscopic diffusion resistance. Especially the molecular sieve effect at the micro-nano scale has unique potential in selective catalysis.

3.3. Sulfur content

Conventional post-modification approaches usually face the fundamental challenge of balancing the high content of functional groups and the large specific surface area of NOPs [112,113]. Specifically, the high polarity and bulky nature of sulfonic acid groups significantly alter surface properties and often lead to pore narrowing or clogging [114]. Therefore, sulfonated NOPs must carefully balance the incorporation of sulfonic acid groups with the preservation of porous structural characteristics to enhance overall material expansion properties [115–117].

Zhu groups proposed that improving the swelling state of NOPs prior to sulfonation was conducive to attaining an optimal balance between specific surface area and sulfur content [118]. The one-pot strategy facilitated the diffusion and modification of the sulfonating reagent throughout the entire porous structure, in the porous aromatic framework (PAF) studied, a specific surface area of 580 m^2/g and a sulfur content of up to 13.2 wt% were achieved, surpassing those of most sulfonated NOPs materials obtained *via* conventional post-sulfonation strategies (Fig. 4a), and significant adsorption capacities for cationic dyes and antibiotics (826–1134 mg/g) were recorded. This strategy has also been confirmed in HCPs and CMPs. Sun *et al.* [119] reported the concentrated sulfonic acid could use for the sulfonication of the HCPs resin at different temperatures, as shown in Fig. 4b, the sulfonation temperature have the distinct effect on the acid capacities of different sulfonic resins. For instance, the sulfonic acid capacities at 70 °C were calculated as 1.94, which is almost three times higher than the 0.79 at 30 °C. Ye and Liu's group reported that the sulfonation time also have effect on the acid content [120], for example, in their case, the hypercrosslinked polystyrnene nanosphere were sulfonated for 12, 18, 24 h (Fig. 4c), respectively. The sulfur atomic percentage of the samples is 2.31 %, 2.43 %, and 2.55 %, respectively, which is consistent with the reaction time proceed. However, in this case the content is not the multiplicative increase. Thus, from an energy efficiency point of view, the appropriate sulfonation time is also a very important choice.

As illustrated in Fig. 4d, Wolska *et al.* [121] found that the positioning and loading of sulfonic acid groups had a significant impact on the catalyst's reactivity in esterification and that both parameters were notably affected by the degree of crosslinking in the polymer matrix. Specifically, sHCP-1, characterized by the lowest degree of crosslinking, tended to be located within the internal pores, exhibited the highest sulfur content (2.22 mmol/g), and yielded the highest conversion of acetic acid, approximately twice that of Amberlyst-15. Sulfonic groups are expected to enhance the separation selectivity between REE^{3+} and Al^{3+}, thereby enabling the effective recovery of trace rare earth elements [122,123]. In the report by Yang *et al.*, the HCP based on the BCMBP monomer achieved a balance between a BET surface area of 1044.6 m^2/g and a sulfur content of 3.27 mmol/g after the introduction of a defined amount of sulfonating agent (designated SHCP-P-3.0) [124], outperforming other monomer types under the same conditions. In actual wastewater, it exhibited high selectivity, with a recovery rate for REE^{3+} of 87 % and an adsorption rate for Al^{3+} of 0 % (Fig. 4e). On the other hand, as illustrated in Fig. 4f, Wolska *et al.* found that a 1 to 4 monomer to sulfonating agent molar ratio, used in the construction of SHCP, retained a high specific surface area (~704 m^2/g) and a high sulfur content (~3.98 mmol/g) [125]. Adsorption equilibrium for ciprofloxacin (~757.7 mg/g) was reached within 3 h outperforming commercial Amberlyst-15 and analogues modified after synthesis, and the material exhibited selective adsorption *via* ionic interactions in complex matrices.

From a catalysis viewpoint, higher sulfur content increases acid site density, thus increasing available catalytic sites in chemical thermodynamics. However, at the same time, the -SO_3H group is large in volume and highly polar, which can easily lead to pore size contraction and inhibit the diffusion of macromolecules or hydrophobic substances, resulting in a decrease in apparent activity.

4. Biodiesel applications

Biodiesel is typically produced *via* transesterification of triglycerides (TG) or esterification of free fatty acids (FFAs) with low molecular weight alcohols, facilitated by appropriate acid or alkaline catalysts. The selection and optimization of catalysts have long been critical challenges in biodiesel production, directly affecting reaction efficiency, product quality, and catalyst recyclability. Although heterogeneous catalysts (*e.g.*, metal oxides, zeolites) exhibit improved stability, their practical application is constrained by insufficient surface area and inadequate exposure of active sites. In recent years, HCPs have emerged as promising candidates in heterogeneous catalysis due to their tunable nanoporous architectures, exceptional surface area, and facile surface functionalization [57,126]. We evaluated the parameters of heterogeneous catalysts (mainly HCPs) from the perspectives of green and sustainability and summarized them in Table S1 (Supporting information).

4.1. Type of catalyst

To improve the post-reaction separation and recyclability of catalysts, extensive efforts have been devoted to exploring heterogeneous catalytic materials as alternatives to homogeneous counterparts. Heterogeneous solid acid catalysts have emerged as promising alternatives to conventional liquid acids (*e.g.*, sulfuric acid, hydrochloric acid) due to the inherent limitations of the latter [127,128]. These solid-phase catalysts not only exhibit high catalytic efficiency but also align with the principles of green chemistry, existing in a stable solid state that circumvents issues such as corrosiveness, separation challenges, and hazardous waste generation associated with their liquid counterparts. Among the developed strategies, direct sulfonation of polymer frameworks has emerged as a simple yet effective approach to introduce catalytically active sulfonic acid groups (-SO_3H) [129–131]. As shown in Fig. S5a (Supporting information), Bhaumik *et al.* innovatively designed three categories of sulfonated pyrene-based porous organic polymers (SPPOPs) [132], strategically utilizing the monomer ratio of bis(1,4-bromomethyl)benzene to pyrene as a "molecular lever" to achieve precise regulation of sulfonation degree and acidic site density. In the work by Wang *et al.*, a sulfonated HCP-based metal-free solid acid was first synthesized. The nano-confinement effect within tailored pore channels significantly enhances catalytic efficiency in bulky-molecule-involved Friedel-Crafts alkylation and the Beckmann rearrangement [44]. Brown *et al.* elucidated the leading role of acid site accessibility in governing catalytic performance for esterification [43]. The D5081 catalyst, featuring a micro-mesoporous hierarchical structure derived from hypercrosslinked networks, demonstrated a nearly 10-fold higher turnover frequency than Amberlyst-15 despite possessing only 21 % of its acid site concentration. Dai *et al.* developed micro–meso–macroporous polymers (MOP) with multifunctional active sites *via in situ* crosslinking of functional molecules like aniline, phloroglucinol, and ethylbenzene with 1,4-bis(chloromethyl)benzene, removing the need for templates [133]. Their MOP-aniline-$[C_4][SO_3CF_3]$ and MOP-ethylbenzene-SO_3H catalysts performed effectively in the

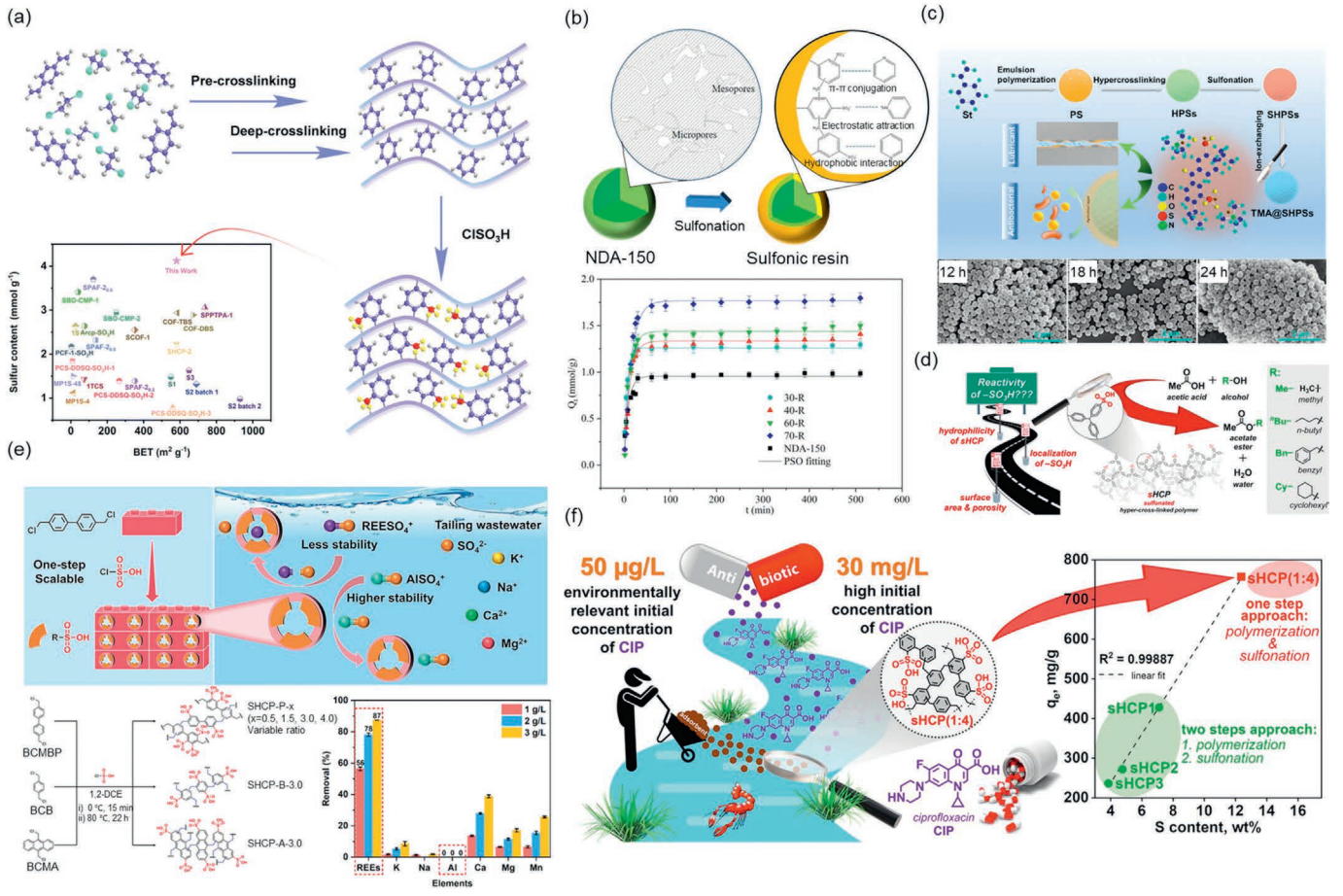


Fig. 4. (a) One-pot synthesis of a highly sulfonated PAF, and comparison of its sulfur content and specific surface area with other sulfonated. Reproduced with permission [118]. Copyright 2025, The Royal Society of Chemistry. (b) Schematic diagram of adsorption mechanism and adsorption kinetic curves of pyridine resins with different degrees of sulfonation. Reproduced with permission [119]. Copyright 2022, Elsevier Publishing Group. (c) Preparation of modified hypercrosslinked polystyrene nanospheres and SEM images of nanospheres with different degrees of sulfonation. Reproduced with permission [120]. Copyright 2024, American Chemical Society. (d) Investigation of factors influencing the reactivity of sulfonic acid groups on HCPs in esterification. Copied with permission [121]. Copyright 2024, Elsevier Publishing Group. (e) Schematic illustration of the scalable synthesis of sulfonic acid-functionalized porous HCPs and the La^{3+} adsorption capacity of SHCP-X in 200 ppm solution. Reproduced with permission [124]. Copyright 2024, Elsevier Publishing Group. (f) Highly sulfonated HCPs enable efficient and selective ciprofloxacin removal from water. Copied with permission [125]. Copyright 2024, Elsevier Publishing Group.

purification of tripalmitin, achieving biodiesel yields of 92.6 % and 86.7 %, respectively, within 14 h, three times higher than Amberlyst −15. While HCPs have emerged as versatile platforms for heterogeneous catalysis in biodiesel production, their applications have predominantly focused on acidic frameworks [134–136]. The exploration of HCPs with tailored basicity remains underexplored, despite the critical role of base catalysts in transesterification reactions [137]. Díaz *et al.* pioneers a mechanochemically synthesized KNO_3-impregnated HCP (HCP-SB-K) as a robust alkaline catalyst for biodiesel production [138]. As shown in Fig. S5b (Supporting information), unlike conventional HCP-based acid catalysts, HCP-SB-K leverages weak basic sites (CO_2-TPD: 2.35 mmol/g, 156 °C) derived from K_2O, achieving exceptional FAME yields (99.9 % for low-FFA oils, 75.9 % for FFA-rich feedstocks) under mild conditions (60 °C, 2 h). However, its limited efficacy for high-FFA oils (>5.83 mg KOH/g) underscores the need for bifunctional HCPs integrating acid-base duality.

In addition to conventional chemical approaches for biodiesel production, the utilization of lipase-catalyzed enzymatic esterification/transesterification has emerged as an environmentally benign and promising alternative methodology [139]. Given the high cost of exogenous lipases employed in biodiesel production, the efficient immobilization of lipases onto ideal carriers (inert polymers and inorganic materials) has been regarded as a promising solution [140]. Current immobilization strategies primarily encompass covalent crosslinking [141,142], adsorption [143–145], entrapment [146,147] and encapsulation [148,149], thereby effectively enhancing enzymatic stability and reusability. A recent breakthrough in enzyme immobilization stability comes from the Wang group [150], who developed a rigid-flexible composite strategy. They constructed a layered material by growing ZIF-8 *in situ* within hydrophobic porous polyvinyl imidazole (Fig. S5c in Supporting information). Defective Zn sites served as coordination-enhanced anchoring points, leading to a remarkable activity recovery (150 %) and a high turnover number. The catalyst remained stable for 44 days, retaining 83 % activity after 16 cycles.

For the treatment of high acid value feedstocks, catalysts with acid-base bifunctional sites are more attractive for their simultaneous conversion, given the need for a complex and expensive two-step process [151]. As depicted in Fig. S5d (Supporting information), Chen *et al.* modified ZIF-67 using phosphotungstic acid (HPW), disrupting the Co-N bonds of ZIF-67 to generate coordinatively unsaturated Co^{2+} and N^- terminal imidazole ligands, thereby enhancing the Lewis acid-base properties of the catalyst [152]. Additionally, the protons introduced with increasing HPW content enhanced the Brønsted acidity, promoting the conversion of microalgal lipids into fatty acid methyl esters. Similarly, enhanced Lewis-Brønsted acid sites also could efficiently catalyze the conversion

of these promising feedstocks. Cheng *et al.* [153] employed sulfamic acid (SA) to modify ZIF–90. The formation of new imine bonds firmly anchored SA to ZIF–90, and the supplied protons disrupted the coordination Zn-N bonds [154], generating unsaturated Zn^{2+} sites (Lewis acid) that promoted TG transesterification, while the -NH groups synergized with SA (Brønsted acid) to facilitate FFA esterification (Fig. S5e in Supporting information). Although both above bifunctional strategies achieved significant results (~98 %), they inevitably must be carried out at high temperatures and pressures (200 °C), and the use of microwaves to further optimize biodiesel production may be explored in future studies [155,156].

It is worth mentioning that the changes in the porosity and morphology of the catalyst largely determine its catalytic activity and reaction efficiency [20,157]. Du *et al.* [158] designed a layered macro–microporous metal–organic framework with tunable dimensions (180–360 nm), which increased enzyme loading by 123.8 %. However, fatty acids induce decomposition of the polymer structure; therefore, as shown in Fig. S5a, template-assisted pyrolysis method was employed to preserve this ordered porous architecture and further improve enzyme loading and catalytic activity. However, the low specific surface area HCP-SB-K (28 m^2/g) also exhibited excellent catalytic activity in biodiesel production (~99.9 % yield) [138]. This performance was attributed to its average pore size (5 nm) being highly matched with the size of TG molecules (5 nm), which allowed the TG to easily penetrate the catalyst pores and ensured effective contact between the reactants and the catalyst surface.

4.2. Different feedstocks

Selection of feedstocks is another critical factor influencing the quality and efficiency of the transesterification process. As biodiesel's role as an alternative to fossil fuels grows, cost reduction and efficiency improvement have become paramount. Research has accordingly expanded to explore a variety of feedstock sources, including single oil feedstocks, such as edible vegetable oils, non-edible vegetable oils, animal fats, waste cooking oils, and algal oils [159], as well as blended feedstocks to overcome the limitations associated with using a single oil source for biodiesel production [160,161]. As illustrated in Fig. S5b, the fatty acid composition and physicochemical properties of these feedstocks vary considerably [162], which in turn affects reaction conditions, catalyst performance, and final product yield [163,164]. Therefore, understanding feedstock characteristics is essential for optimizing process parameters and ensuring consistent biodiesel production [165]. A detailed discussion of the various feedstocks characteristics and their impact on the production process can be found in Text S4.2 (Supporting information).

4.3. Reaction conditions

The reaction conditions for biodiesel production are explored in detail, which can be found in Text S4.3 (Supporting information).

4.4. Intelligent management

The synthesis of hierarchical nanoporous polymers with controlled morphologies remains challenging, often relying on complex templating strategies [130]. Song *et al.* proposed an assembly strategy mediated by Lewis acid–base interactions and successfully synthesized HHNP-B, a polymer with a rigid hollow framework and intrinsic hydroxyl functionalities. Subsequent sulfonation with concentrated H_2SO_4 yielded SHNP-B, which served as a heterogeneous solid acid catalyst [81]. Under mild conditions (25 °C, 6 h), SHNP-B achieved high conversion rates (>91.6 %) for most esterification substrates. In contrast, sulfonated irregular solid-spherical HCPs exhibited significantly lower yields (65.6 %), highlighting the structural advantages of HHNP-B in catalytic performance. Notably, the Box-Behnken response surface methodology (RSM) was employed to evaluate the relationship between variables and responses [166,167], which determined the optimal conditions for oil transesterification using the SHNP catalyst (reaction time: 10.5 h; methanol/oil weight ratio: 34.35; reaction temperature: 70 °C) and achieved high conversion rates (~90 % yield) for most substrates.

Poly(ionic liquid)s (PILs), which feature repeating ionic liquid groups integrated within a polymer network, have attracted considerable interest for their potential applications across diverse fields [99,168–170]. In Yang *et al.*'s work, a [DSI][$FeCl_4$] catalyst featuring both Brønsted and Lewis acidic sites was synthesized by a simple and atom-economic route, a highly porous structure can be observed in both SEM and TEM images, and it achieved the efficient conversion of non-edible *Firmiana platanifolia* (L. f.) oil to biodiesel (Fig. S7a in Supporting information) [171]. Its high acid density (3.73 mmol/g) and mesoporous structure significantly enhanced the mass transfer of reactants. Under the RSM-optimized conditions (120 °C, 10–11 h, methanol-to-oil molar ratio of 25:1), the use of biomass-derived tetrahydrofuran improved the miscibility between oil and methanol, resulting in a biodiesel yield of 98.7 % that was superior to conventional commercial resins. This has provided a paradigm for customizing ionic solid acids to realize sustainable biorefining processes. Qiu and coworkers were the first to employ the economical and renewable raw material Sapindus oil for biodiesel production (Fig. S7b in Supporting information) [172]. The designed PIL microsphere catalyst is distinct from traditional PIL nanoparticles, featuring a unique cross-linked microsphere structure (500 μm in diameter) that combines exceptional mechanical strength and hierarchical porosity (specific surface area of 100.1 m^2/g and mesopore diameter of 18.9 nm), addressing critical limitations in catalyst recovery and mass transfer. The hydrophobic-oleophilic balance of the material selectively enriches reactants at the active sites, achieving a 95.2 % FAME yield from Sapindus oil under optimized conditions determined by response surface methodology. Furthermore, some studies have shown that incorporating metal chlorides or metal sulfates into Brønsted acidic ionic liquids enables the catalysts to possess both Brønsted and Lewis acidic sites [173]. Qiu *et al.* demonstrated a rational design strategy for Brønsted-Lewis acidic ILs *via* a synergistic computational and experimental approach. The integrated use of electrostatic potential analysis and proton affinity calculations precisely selected 4–methylthiazole as the optimal substrate, and $FeCl_3$ was subsequently introduced to enhance Lewis acidity, thereby generating a synergistic catalytic effect. In their orthogonal experiments and response surface optimizations, [PS–MTH][CF_3SO_3]–$FeCl_3$ (mole fraction of metal chloride = 0.65) exhibited the best catalytic performance (~97.04 % yield, Fig. S7c in Supporting information) [174]. In a recent report, Kachhwaha and coworkers employed a novel high-speed homogenizer-assisted process intensification technique to synthesize biodiesel from high FFA (80.65 %) soya acid oil, marking a breakthrough in this field (Fig. S7d in Supporting information) [175]. Through Box–Behnken optimization, determine its optimal conditions: a methanol-to-oil ratio of 18.4:1, a reaction time of 84.6 min, 2.18 wt% catalyst, and a rotational speed of 14,100 RPM, they achieved a significant 98.06 % conversion of FFAs, thereby demonstrating higher efficiency than conventional mechanical stirring. Notably, the biodiesel produced by this process complies with EN 14,214, thus maintaining commercial viability. The use of used cooking oil (UCO) for biodiesel production is essential to move towards carbon neutrality [176]. Recently, Atray *et al.* utilized a novel solvent as both a phase-transfer agent and a demulsifier to achieve the efficient conver-

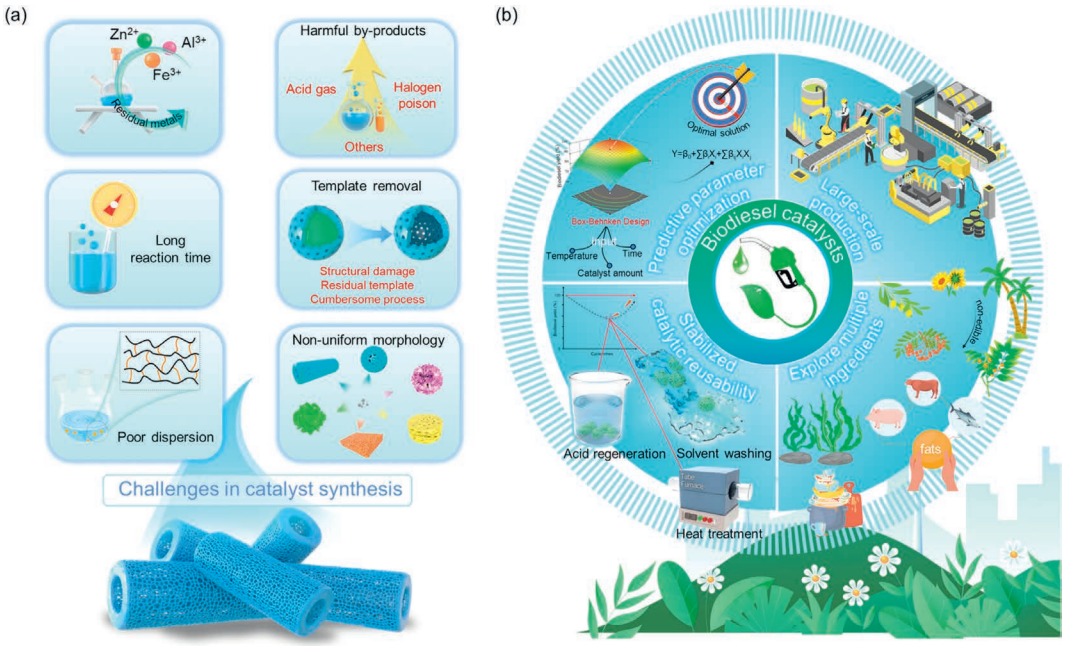


Fig. 5. (a) Challenges in the synthesis of hypercrosslinked polymers. (b) Prospects for the application of biodiesel production.

sion of UCO at room temperature [177]. The proposed "distributed drive model" embedded production units into rural or peri–urban settings, thereby directly connecting UCO suppliers with end users and combining technical feasibility with economic advantages. Al-Hamamre *et al.* innovatively exploited the structural complexity of lignin to modulate the architecture of sulfonated carbon aerogels through sol–gel synthesis and chemical activation (Fig. S7e in Supporting information) [178]. Unlike conventional activation methods, the sol-gel approach produced a hierarchical pore network (with a surface area of 78.1 m^2/g and an acid density of 2.81 mmol/g), which enabled a biodiesel conversion of 96.58 % from waste oil, performance that surpassed most biomass-derived catalysts. Although the reusability of the catalysts remained constrained by sulfur leaching, the integration of response surface methodology and multi-scale characterization has provided a blueprint for optimizing porous catalyst systems. Traditional statistical methods such as RSM are widely used to optimize production processes, especially in experimental design and analysis under the influence of multiple variables. However, as data complexity has increased, these methods have been shown to encounter limitations when dealing with nonlinear and high-dimensional datasets. In recent years, artificial neural networks (ANNs) have garnered increasing attention in the field of biodiesel due to their powerful nonlinear mapping capabilities and their flexibility in adapting to complex data [178–181]. Hosseinpour and coworkers innovatively combined the dimension reduction advantages of partial least squares (PLS) for handling high-dimensional data with the nonlinear mapping ability of ANN to enhance prediction accuracy (Fig. S7f in Supporting information), associating the biodiesel cetane number with the FAME curve and thereby overcoming the limitations of traditional linear PLS in modeling nonlinear systems [182]. By integrating an artificial neural network to optimize latent variable relationships, the hybrid model achieved excellent accuracy ($R^2 > 0.99$) in 135 biodiesel samples, outperforming standalone PLS ($R^2 \approx 0.85$). Although this study demonstrated the transformative potential of machine learning in optimizing fuel properties, its reliance on historical data raises questions regarding its generalizability to new feedstocks. Nevertheless, this framework has provided a template for predicting multifunctional characteristics in complex bio-based systems, representing a crucial step toward data-driven biodiesel design.

5. Conclusions and perspectives

Bio-renewable energy is fast becoming the cornerstone of sustainable energy solutions, radically reducing dependence on finite fossil fuels while mitigating environmental impacts. Biodiesel is one of the most sustainable and green liquid fuels from biomass and is considered a renewable, biodegradable, environmentally friendly and non-toxic fuel from edible/non-edible feedstocks. Advanced heterogenous catalytic materials show promising applications in catalysing transesterification and esterification reactions for biodiesel preparation due to their high catalytic activity, corrosion resistance, ease of recycling, easy availability of resources, and high designability of the active sites. In particular, the synergistic effect of the new HCP catalysts developed by combining the multifunctional synthesis strategy with the principles of green chemistry and the process enhancement is expected to further advance the bio refining methods, paving the way for an industrially scalable, economically viable and environmentally friendly biodiesel production pathway. Remarkably, the intelligent manufacturing has made the biodiesel industry more efficient and effective.

Although HCPs have shown broad application prospects with the significant progress made in recent years in the fields of reaction condition optimisation, multifunctional monomer design, structure optimisation and polymerisation strategies, there are still many technical difficulties to be overcome in achieving high-performance synthesis, large-scale production and environmentally friendly preparation. As depicted in Fig. 5a, these challenges necessitate consideration for further development: (1) Conventional HCPs synthesis relies on metal-based Lewis acid catalysts, which are difficult to remove completely after the reaction, residual metal ions may contaminate the product and the post-treatment step is time-consuming. Although metal-free catalyst systems, such as Bronsted acid have been developed, but there is also a need to avoid the occurrence of side reactions, the side effect on the porosity also need to be addressed; (2) Halogen-containing monomers or cross-linkers inevitably produce harmful by-products

after cross-linking. Although preliminary explorations on halogen-free systems have been undertaken, the development of improved halogen-free materials that combine environmental friendliness with competitive performance remains a core challenge in this field; (3) The traditional hypercrosslinking process requires a reaction time of at least 24 h, which significantly restricts production efficiency. To overcome this bottleneck, researchers have developed techniques such as mechanical ball milling, continuous flow synthesis, and microwave-assisted synthesis that reduce the reaction time to 5–60 min; (4) Morphological control relies on templating methods. Hard templates (*e.g.*, SiO_2) require HF etching, while soft templates (*e.g.*, block copolymers) involve tedious synthetic steps. The template free methods still in the laboratory preparation stage. Therefore, there is an urgent need for a simple, universally applicable, and scalable strategy; (5) The Friedel-Crafts reaction, due to its rapid and stochastic nature, leads to irregularities and agglomerations of the HCPs, limiting their dispersion and hindering their potential in various heterogeneous catalytic applications. In response, researchers have typically used restricted cross-linking strategies or hydrophilic group grafting to improve dispersibility.

After identifying the five challenges mentioned above, as shown in Fig. 5b, the next section will focus on the four major prospects shown in biodiesel production and explore new opportunities for its green and efficient preparation: (1) In recent years, in order to alleviate ethical controversies over the competition between food and fuel and to reduce dependency on fossil resources, the biodiesel feedstock system has gradually expanded from first-generation edible vegetable oils (*e.g.*, soybean and canola oils) to non-edible lipid resources, including oils from marginal land crops, waste animal and vegetable fats, microbially derived lipids, and diversified carbon sources derived from industrial and municipal by-products. This transformation in feedstock composition not only conforms to the principles of a low-carbon circular economy but also provides new avenues for overcoming the bottlenecks associated with conventional raw material supplies; (2) During continuous catalytic cycles in biodiesel production, effective catalyst regeneration becomes imperative to sustain long-term process efficiency. To restore catalytic activity, several regeneration strategies have been implemented. Acid regeneration generally employs chemical treatments (*e.g.*, reintroducing -SO_3H groups) to restore the acidic sites diminished due to leaching or blockage by impurities. Its future development should focus on three major objectives: enhancing regeneration efficiency, reducing environmental burdens, and extending catalyst lifespan. Secondly, solvent washing usually uses organic solvents such as methanol and acetone to dissolve hydrophobic deposits such as glycerol and saponification on the surface and restore the mass transfer channels. Future developments are expected to focus on optimising solvent efficiency and process reliability to further consolidate its role in catalyst regeneration; (3) Biodiesel production performance is influenced by the interactions among multiple factors, such as temperature, catalyst loading, and the methanol-to-oil ratio, and traditional one-variable experiments are inadequate for revealing complex nonlinear relationships. RSM as a commonly used optimization tool, effectively explores the interactions among these factors through systematic experimental design. Among the various RSM approaches, the Box–Behnken design (BBD) is widely adopted owing to its reduced number of experiments and high predictive accuracy. In the future, by integrating machine learning, multi-objective optimization, and high-throughput technologies, BBD will further drive the transformation of catalyst design from an "empirical trial-and-error" approach to a "data-driven" intelligent paradigm, thereby providing a reliable theoretical basis for the industrialization of biodiesel; (4) In the green transition and expansion of the biodiesel industry, large-scale production has become essential to meet growing market demand and to advance a low-carbon circular economy. Continuous-flow reactors are increasingly replacing batch reactors, enhancing reaction efficiency and uniformity. Real-time monitoring systems and automated control technologies enable dynamic adjustment of critical process parameters, thereby ensuring stable and efficient production. Modular process design integrates all stages, from pretreatment and reaction to separation and waste management, reducing costs and offering greater flexibility for scaling up. Waste heat recovery and process integration improve energy efficiency and reduce emissions. In addition, exploring moulding methods such as electrospinning [183–186], 3D printing [187] and coatings [188] can further expand the scenarios in which HCPs catalysts can be used and unlock their full green potential. Overall, the coordinated development of technological innovation and various segments of the industrial chain has been propelling the large-scale production of biodiesel toward a greener, smarter, and more efficient future.

Declaration of competing interest

The authors declare that they have no known competing financial interests or personal relationships that could have appeared to influence the work reported in this paper.

CRediT authorship contribution statement

Yuheng Wen: Writing – review & editing, Writing – original draft, Visualization, Methodology, Investigation, Formal analysis, Conceptualization. **Zeyu Wang:** Writing – original draft, Visualization, Methodology, Formal analysis, Conceptualization. **Jingli Li:** Writing – review & editing, Writing – original draft, Investigation. **Chengyao Xue:** Writing – review & editing, Writing – original draft, Investigation. **Haobo Wang:** Writing – original draft, Investigation, Conceptualization. **Xingrui Li:** Writing – original draft, Investigation, Conceptualization. **Hao Zhang:** Writing – original draft, Investigation, Conceptualization. **Yang Lu:** Writing – review & editing, Investigation, Funding acquisition, Conceptualization. **Yu Zhang:** Writing – review & editing, Formal analysis, Data curation, Conceptualization. **Qing Hou:** Writing – review & editing, Supervision, Investigation, Funding acquisition. **Wenliang Song:** Writing – review & editing, Writing – original draft, Resources, Methodology, Investigation, Funding acquisition, Formal analysis, Conceptualization.

Acknowledgments

The research work was supported by sponsored by Natural Science Foundation of Shanghai (No. 25ZR1402392). The authors acknowledge funding from the National Natural Science Foundation of China (No. 52401057).

Supplementary materials

Supplementary material associated with this article can be found, in the online version, at doi:10.1016/j.cclet.2025.111960.

References

[1] Y. Guan, J. Yan, Y. Shan, et al., Nature Energy 8 (2023) 304–316.
[2] T.A. Shaw, B. Stevens, Nature 639 (2025) 877–887.
[3] S. Zhou, B. Yu, Y. Zhang, Sci. Adv. 9 (2023) eabo1638.
[4] Y. Geng, Y. Liu, P. Li, et al., Sci. Adv. 11 (2025) eads4355.
[5] A. Lal, F. You, Sci. Adv. 9 (2023) eadg6740.
[6] J. Kim, S. Ravi, K. Kim, et al., ACS Appl. Mater. Interfaces 15 (2023) 48485–48494.
[7] K.F. Pfister, S. Baader, M. Baader, S. Berndt, L.J. Goossen, Sci. Adv. 3 (2017) e1602624.
[8] R.H. Moore, K.L. Thornhill, B. Weinzierl, et al., Nature 543 (2017) 411–415.
[9] O. Filip, K. Janda, L. Kristoufek, D. Zilberman, Nature Energy 1 (2016) 16169.
[10] R.C. Rial, Renew. Sustain. Energy Rev. 196 (2024) 114369.

[11] A.I. Osman, M. Nasr, M. Farghali, et al., Environ. Chem. Lett. 22 (2024) 1005–1071.
[12] S. Sikiru, K.J. Abioye, H.B. Adedayo, et al., Renew. Sustain. Energy Rev. 200 (2024) 114535.
[13] L. He, L.L. Zhang, H. Zhou, et al., Adv. Energy Mater. 15 (2025) 2403168.
[14] T. Suthisripok, P. Semsamran, Tribol. Int. 128 (2018) 397–409.
[15] A.K. Agarwal, T. Gupta, A. Kothari, Renew. Sustain. Energy Rev. 15 (2011) 3278–3300.
[16] M. Jamshaid, H.H. Masjuki, M.A. Kalam, et al., Energy 239 (2022) 121894.
[17] P. Rosha, S.K. Mohapatra, S.K. Mahla, et al., Energy 178 (2019) 676–684.
[18] A. Cheruvathoor Poulose, M. Medveď, V.R. Bakuru, et al., Nat. Commun. 14 (2023) 1373.
[19] J. Liu, R. Burciaga, S. Tang, et al., Innov. Mater. 2 (2024) 100090.
[20] A.F. Lee, J.A. Bennett, J.C. Manayil, K. Wilson, Chem. Soc. Rev. 43 (2014) 7887–7916.
[21] L. He, L. Chen, Y. Nie, et al., Green Chem. 26 (2024) 5954–5965.
[22] Q. Wu, Fuel 332 (2023) 126132.
[23] F. Su, Y. Guo, Green Chem. 16 (2014) 2934–2957.
[24] W. Gong, Y. Liu, H. Li, Y. Cui, Coord. Chem. Rev. 420 (2020) 213400.
[25] C.O. Tuck, E. Pérez, I.T. Horváth, R.A. Sheldon, M. Poliakoff, Science 337 (2012) 695–699.
[26] M. Hara, Energy Environ. Sci. 3 (2010) 601–607.
[27] J. Liu, Y. Nan, L.L. Tavlarides, Fuel 193 (2017) 187–196.
[28] X. Chen, H. Jiang, X. Li, et al., Angew. Chem. Int. Ed. 58 (2019) 14748–14757.
[29] F. Ursino, G. Mineo, A. Scandurra, et al., Nano Res. 17 (2024) 9585–9593.
[30] C.M. Friend, B. Xu, Acc. Chem. Res. 50 (2017) 517–521.
[31] A. Corma, H. García, Chem. Rev. 103 (2003) 4307–4366.
[32] M. Gao, L. Wang, Y. Yang, et al., ACS Catal. 13 (2023) 4060–4090.
[33] J.K. Nørskov, T. Bligaard, B. Hvolbæk, et al., Chem. Soc. Rev. 37 (2008) 2163–2171.
[34] A.H. Jenkins, J.W. Medlin, Acc. Chem. Res. 54 (2021) 4080–4090.
[35] J.C. Védrine, Chin. J. Catal. 40 (2019) 1627–1636.
[36] M. Debruyne, V. Van Speybroeck, P. Van Der Voort, C.V. Stevens, Green Chem. 23 (2021) 7361–7434.
[37] X. Gao, B. Zheng, X. Cao, L. Li, H. Ren, Innov. Mater. 3 (2025) 100117.
[38] X. Luo, J. Luo, J.T. Lin, G.H. Ning, D. Li, Innov. Mater. 2 (2024) 100087.
[39] D. Wu, H. Wang, Y. Nie, et al., Prog. Mater. Sci. 155 (2026) 101538.
[40] Z. Liu, R. Wang, J. Yu, et al., Nano Res. 17 (2024) 9679–9687.
[41] L. Tan, B. Tan, Chem. Soc. Rev. 46 (2017) 3322–3356.
[42] W. Song, Y. Tang, B.Y. Moon, et al., Green Chem. 26 (2024) 2476–2504.
[43] E. Andrijanto, E.A. Dawson, D.R. Brown, Appl. Catal. B 115-116 (2012) 261–268.
[44] J. Li, X. Wang, G. Chen, et al., Appl. Catal. B 176-177 (2015) 718–730.
[45] Z. Jia, K. Wang, B. Tan, Y. Gu, ACS Catal. 7 (2017) 3693–3702.
[46] S. Mondal, J. Mondal, A. Bhaumik, ChemCatChem 7 (2015) 3570–3578.
[47] X. Liu, L. Yu, G. Zhu, et al., Nano Res. 17 (2024) 9857–9864.
[48] A.M. Borrero-López, A. Celzard, V. Fierro, ACS Sustainable Chem. Eng. 10 (2022) 16090–16112.
[49] E.O. Pyzer-Knapp, J.W. Pitera, P.W.J. Staar, et al., npj Comput. Mater. 8 (2022) 84.
[50] C. López, Adv. Mater. 35 (2023) 2208683.
[51] V. Davankov, M. Tsyurupa, Chapter 6 - Preparation of macronet isoporous and hypercrosslinked polystyrene networks, in: V.A. Davankov, M.P. Tsyurupa (Eds.), Comprehensive Analytical Chemistry, Elsevier, 2011, pp. 166–193.
[52] V.A. Davankov, S.V. Rogoshin, M.P. Tsyurupa, J. Polym. Sci. 47 (1974) 95–101.
[53] Y. Ahmadi, K.H. Kim, Polym. Rev. 63 (2023) 365–393.
[54] T.A. Makal, J.R. Li, W. Lu, H.C. Zhou, Chem. Soc. Rev. 41 (2012) 7761–7779.
[55] Z. Cai, X. Hu, Z.a. Li, et al., Water Res. 227 (2022) 119341.
[56] Y. Su, Z. Wang, A. Legrand, et al., J. Am. Chem. Soc. 144 (2022) 6861–6870.
[57] J.Y. Jang, Y.K. Kim, Y.J. Ko, S.U. Son, ACS Sustainable Chem. Eng. 12 (2024) 8880–8889.
[58] W. Song, Y. Zhang, D.G. Yu, et al., Biomacromolecules 22 (2021) 732–742.
[59] Y. Zhang, Y. Wu, Y. Fu, Q.X. Jia, Z. Zhang, Sens. Actuators B 401 (2024) 134997.
[60] J. Liu, W. Duan, J. Song, et al., J. Am. Chem. Soc. 141 (2019) 12064–12070.
[61] J.S.M. Lee, M.E. Briggs, T. Hasell, A.I. Cooper, Adv. Mater. 28 (2016) 9804–9810.
[62] W. Song, Y. Wen, Z. Wang, et al., Langmuir 40 (2024) 16670–16689.
[63] W. Song, Y. Zhang, A. Varyambath, J.S. Kim, I. Kim, Green Chem. 22 (2020) 3572–3583.
[64] N. Fontanals, R.M. Marcé, F. Borrull, P.A.G. Cormack, Polym. Chem. 6 (2015) 7231–7244.
[65] J. Sawada, D. Aoki, Y. Sun, K. Nakajima, T. Takata, ACS Appl. Polym. Mater. 2 (2020) 1061–1064.
[66] L.J. Abbott, C.M. Colina, Macromolecules 47 (2014) 5409–5415.
[67] J. Huang, R. Deng, K. Huang, Chem. Eng. J. 171 (2011) 951–957.
[68] F. Gao, R. Bai, M. Li, Y. Gu, Green Chem. 23 (2021) 7499–7505.
[69] A. Hao, Z. Fu, J. Huang, Sep. Purif. Technol. 311 (2023) 123380.
[70] C. Wilson, M.J. Main, N.J. Cooper, et al., Polym. Chem. 8 (2017) 1914–1922.
[71] V.A. Davankov, M.P. Tsyurupa, React. Polym. 13 (1990) 27–42.
[72] K. Schute, M. Rose, ChemSusChem 8 (2015) 3419–3423.
[73] C. Detoni, C.H. Gierlich, M. Rose, R. Palkovits, ACS Sustainable Chem. Eng. 2 (2014) 2407–2415.
[74] X. Wu, Y. Liu, Y. Liu, et al., RSC Adv. 5 (2015) 72601–72609.
[75] X. Zhao, X. Wang, J. Yan, J. Appl. Polym. Sci. 92 (2004) 997–1004.
[76] X. Tang, J. Wei, J. Yan, J. Appl. Polym. Sci. 94 (2004) 2041–2049.
[77] S. Mane, S. Ponrathnam, N. Chavan, Eur. Polym. J. 59 (2014) 46–58.
[78] J. Wei, X.Y. Bai, J. Yan, Macromolecules 36 (2003) 4960–4966.
[79] T.N. Gao, T. Wang, W. Wu, et al., Adv. Mater. 31 (2019) 1806254.
[80] Y. Zhang, S. Li, Y. Xu, et al., Nano Res. 15 (2022) 5556–5568.
[81] W. Song, Y. Zhang, A. Varyambath, I. Kim, ACS Nano 13 (2019) 11753–11769.
[82] V.G. Snider, R. Alshehri, R.M. Slaugenhaupt, C.L. Hill, ACS Appl. Mater. Interfaces 13 (2021) 51519–51524.
[83] N. Saini, A. Malik, S.L. Jain, Coord. Chem. Rev. 502 (2024) 215636.
[84] P. Tyagi, D. Singh, N. Malik, S. Kumar, R. Singh Malik, Mater. Today 65 (2023) 133–165.
[85] Sahil, N. Gupta, Renew. Sustain. Energy Rev. 193 (2024) 114297.
[86] Y.L. Wan, L. Wang, L. Wen, J. CO_2 Util. 64 (2022) 102174.
[87] X. Wang, S. Ma, B. Chen, et al., Green Energy Environ. 5 (2020) 138–146.
[88] Y. Zhang, B. Wang, E.H.M. Elageed, et al., ACS Macro Lett. 5 (2016) 435–438.
[89] G. Celik, S.A. Ailawar, H. Sohn, et al., ACS Catal. 8 (2018) 6796–6809.
[90] Y. Xu, Y. Yao, H. Yu, et al., ACS Macro Lett. 8 (2019) 1263–1267.
[91] K. Lee, N. Corrigan, C. Boyer, Angew. Chem. Int. Ed. 62 (2023) e202307329.
[92] M. Seo, S. Kim, J. Oh, S.-J. Kim, M.A. Hillmyer, J. Am. Chem. Soc. 137 (2015) 600–603.
[93] X. Li, J. Gu, Z. Hong, et al., J. Membr. Sci. 722 (2025) 123910.
[94] J. Wang, T. Wu, D. Li, et al., Sep. Purif. Technol. 340 (2024) 126833.
[95] W. Wang, Z. Wang, X. Sun, Z. Yi, C. Gao, J. Membr. Sci. 707 (2024) 122990.
[96] W. Wang, Z. Shu, H. Wei, et al., Small 20 (2024) 2308171.
[97] M.P. Tsyurupa, V.A. Davankov, React. Funct. Polym. 53 (2002) 193–203.
[98] M.P. Tsyurupa, V.A. Davankov, React. Funct. Polym. 66 (2006) 768–779.
[99] S. Yang, Z. Zhong, J. Hu, X. Wang, B. Tan, Adv. Mater. 36 (2024) 2307579.
[100] D. Schneider, D. Mehlhorn, P. Zeigermann, J. Kärger, R. Valiullin, Chem. Soc. Rev. 45 (2016) 3439–3467.
[101] M.R. Benzigar, S.N. Talapaneni, S. Joseph, et al., Chem. Soc. Rev. 47 (2018) 2680–2721.
[102] J. Yang, H. Wu, M. Zhu, et al., Nano Energy 33 (2017) 453–461.
[103] D. Liu, D. Zou, H. Zhu, J. Zhang, Small 14 (2018) 1801454.
[104] S. Liu, J. Ren, H. Zhang, et al., J. Catal. 335 (2016) 11–23.
[105] X.Y. Yang, L.H. Chen, Y. Li, et al., Chem. Soc. Rev. 46 (2017) 481–558.
[106] S. Yang, S. Wang, X. Liu, L. Li, Carbon 147 (2019) 540–549.
[107] S. Yu, G.L. Xing, L.H. Chen, T. Ben, B.L. Su, Adv. Mater. 32 (2020) 2003270.
[108] N. Zhang, F. Liu, S.D. Xu, et al., J. Mater. Chem. A 5 (2017) 22631–22640.
[109] S. Israel, M. Levin, S. Oliel, et al., Macromolecules 55 (2022) 1992–2002.
[110] Y. Xu, T. Wang, Z. He, et al., Appl. Catal. A 541 (2017) 112–119.
[111] J. Hu, H. Gao, X. Wang, B. Tan, Adv. Mater. 37 (2025) 2418005.
[112] X. Wei, X. Jiang, J. Wei, S. Gao, Chem. Mater. 28 (2016) 445–458.
[113] Y. Zhang, S.N. Riduan, Chem. Soc. Rev. 41 (2012) 2083–2094.
[114] J. Zhang, K. Dong, W. Luo, H. Guan, Fuel 234 (2018) 664–673.
[115] K. Zong, K. Jiang, X. Bao, D. Deng, J. Environ. Chem. Eng. 13 (2025) 116082.
[116] X. Liu, J. Wang, Y. Shang, C.T. Yavuz, N.M. Khashab, J. Am. Chem. Soc. 146 (2024) 2313–2318.
[117] W. Zou, G. Jiang, W. Zhang, et al., Adv. Funct. Mater. 33 (2023) 2213642.
[118] L. Yang, Z. Zhan, L. Zhao, et al., Chem. Sci. 16 (2025) 775–783.
[119] Y. Sun, Y. Gu, J. Yang, Chem. Eng. J. 428 (2022) 131163.
[120] Y. Wang, S. Wu, K. Yan, et al., Langmuir 40 (2024) 8992–9000.
[121] J. Wolska, L. Wolski, Arabian J. Chem. 17 (2024) 105600.
[122] M. Hermassi, M. Granados, C. Valderrama, et al., J. Cleaner Prod. 379 (2022) 134742.
[123] M. Traore, A. Gong, Y. Wang, et al., J. Rare Earths 41 (2023) 182–189.
[124] S. Liang, Q. Meng, Z. Liu, et al., Chem. Eng. J. 499 (2024) 155850.
[125] J. Wolska, M. Frankowski, J. Jenczyk, L. Wolski, Sep. Purif. Technol. 343 (2024) 127147.
[126] B. Jiang, J. Liu, W. Xiong, et al., Chem. Eng. J. 476 (2023) 146873.
[127] J.Y. Park, Z.M. Wang, D.K. Kim, J.S. Lee, Renew. Energy 35 (2010) 614–618.
[128] C.H. Su, Appl. Energy 104 (2013) 503–509.
[129] W. Lu, D. Yuan, J. Sculley, et al., J. Am. Chem. Soc. 133 (2011) 18126–18129.
[130] Q. Sun, Z. Dai, X. Meng, F.S. Xiao, Chem. Soc. Rev. 44 (2015) 6018–6034.
[131] P. Schweng, D. Guerin-Faucheur, F. Kleitz, R.T. Woodward, Chem. Commun. 60 (2024) 14395–14398.
[132] S.K. Kundu, A. Bhaumik, ACS Sustainable Chem. Eng. 3 (2015) 1715–1723.
[133] F. Liu, C. Liu, W. Kong, et al., Green Chem. 18 (2016) 6536–6544.
[134] Q. Ao, L. Jiang, J. Tang, Carbohydr. Polym. 357 (2025) 123457.
[135] S.P. Gouda, D. Shi, S. Basumatary, et al., Chem. Eng. J. 480 (2024) 148154.
[136] K. Xiao, Z. Zhou, C. Ye, J. Chen, T. Qiu, Chem. Eng. J. 478 (2023) 147398.
[137] X.X. Yang, Y.T. Wang, Y.T. Yang, et al., Energy Convers. Manage. 164 (2018) 112–121.
[138] S. Señorans, E. Rangel-Rangel, E.M. Maya, L. Díaz, React. Funct. Polym. 202 (2024) 105964.
[139] J.H.C. Wancura, M. Brondani, M.S.N. dos Santos, et al., Renew. Energy 216 (2023) 119085.
[140] M.M. Zheng, Y. Lu, F.H. Huang, et al., J. Agric. Food Chem. 61 (2013) 231–237.
[141] X. Cao, H. Xu, F. Li, et al., Renew. Energy 171 (2021) 11–21.
[142] L. Zhong, X. Jiao, H. Hu, et al., Renew. Energy 171 (2021) 825–832.
[143] E. Navarro López, A. Robles Medina, P.A. González Moreno, et al., Bioresour. Technol. 187 (2015) 346–353.
[144] M. Adnan, K. Li, J. Wang, L. Xu, Y. Yan, Int. J. Mol. Sci. 19 (2018) 1424.
[145] I. Hasnaoui, S. Mechri, A. Dab, et al., Molecules 30 (2025) 434.
[146] B.S. Heater, Z. Yang, M.M. Lee, M.K. Chan, J. Am. Chem. Soc. 142 (2020) 9879–9883.
[147] D. Kumar, T. Das, B.S. Giri, B. Verma, Renew. Energy 147 (2020) 11–24.
[148] F. Zha, M. Shi, H. Li, J. Rao, B. Chen, Fuel 357 (2024) 129854.
[149] R. Al-Mansouri, W. Du, S. Al-Zuhair, Fuel 311 (2022) 122630.
[150] Q. Wang, X. Zheng, M. Ge, et al., Chem. Eng. J. 511 (2025) 162208.
[151] B. Zheng, L. Ban, Y. Nie, et al., J. Cleaner Prod. 453 (2024) 142263.

[152] J. Cheng, H. Guo, X. Yang, et al., Energy Convers. Manage. 232 (2021) 113872.
[153] Y. Mao, J. Cheng, H. Guo, et al., Fuel 331 (2023) 125795.
[154] N. Pan, L. Li, J. Ding, et al., J. Colloid Interface Sci. 508 (2017) 303–312.
[155] Y. Shen, Q. Zhang, X. Sun, et al., Energy Convers. Manage. 286 (2023) 117022.
[156] A.A. Arpia, W.H. Chen, S.S. Lam, P. Rousset, M.D.G. de Luna, Chem. Eng. J. 403 (2021) 126233.
[157] H. Zhang, H. Li, C.C. Xu, S. Yang, ACS Catal. 9 (2019) 10990–11029.
[158] H. Zhou, Z. Zou, L. Dai, D. Liu, W. Du, ACS Sustainable Chem. Eng. 10 (2022) 14503–14514.
[159] K. Srikumar, Y.H. Tan, J. Kansedo, et al., Biomass Bioenergy 185 (2024) 107239.
[160] S. Brahma, B. Nath, B. Basumatary, et al., Chem. Eng. J. Adv. 10 (2022) 100284.
[161] S. Brahma, B. Basumatary, S.F. Basumatary, et al., Fuel 336 (2023) 127150.
[162] S.K. Hoekman, A. Broch, C. Robbins, E. Ceniceros, M. Natarajan, Renew. Sustain. Energy Rev. 16 (2012) 143–169.
[163] E.K. Sitepu, K. Heimann, C.L. Raston, W. Zhang, Renew. Sustain. Energy Rev. 123 (2020) 109762.
[164] V. Praveena, L.J. Martin, J. Matijošius, et al., Renew. Sustain. Energy Rev. 192 (2024) 114178.
[165] R.M.N. Kalla, M.-R. Kim, I. Kim, Ind. Eng. Chem. Res. 57 (2018) 11583–11591.
[166] J. Gupta, M. Agarwal, A.K. Dalai, Renew. Energy 134 (2019) 509–525.
[167] P.M. Veiga, A.S. Luna, M. de Figueiredo Portilho, C. de Oliveira Veloso, C.A. Henriques, Energy 75 (2014) 453–462.
[168] Q. Li, W. Li, Z. Liu, et al., Adv. Mater. 36 (2024) 2311214.
[169] Y. Li, T. Van Cleve, R. Sun, et al., ACS Energy Lett. 5 (2020) 1726–1731.
[170] B. Pei, X. Xiang, T. Liu, et al., Catalysts 9 (2019) 963.
[171] H. Pan, H. Li, H. Zhang, et al., Energy Convers. Manage. 166 (2018) 534–544.
[172] Y. Feng, L. Li, X. Wang, J. Yang, T. Qiu, Energy Convers. Manage. 153 (2017) 649–658.
[173] F. Guo, Z. Fang, X.F. Tian, Y.D. Long, L.Q. Jiang, Bioresour. Technol. 102 (2011) 6469–6472.
[174] D. Cai, Y. Xie, L. Li, et al., Energy Convers. Manage. 166 (2018) 318–327.
[175] N. Prajapati, S. Singh Kachhwaha, P. Kodgire, R. Kumar Vij, Energy Convers. Manage. 324 (2025) 119302.
[176] P. Yang, Q. Chen, W. Xu, et al., Energy Convers. Manage. 325 (2025) 119354.
[177] A.K. Bhonsle, A. Kumar, A. Ray, et al., Energy Convers. Manage. 324 (2025) 119282.
[178] Z. Al-Hamamre, M. Alnaief, J. Yamin, et al., Energy Convers. Manage. 325 (2025) 119381.
[179] Y. Yang, D. Jiang, Q. Zhang, et al., BME Front. 4 (2023) 0030.
[180] G. Wang, BME Front. 5 (2024) 0036.
[181] D. Amsterdam, BME Front. 4 (2023) 0033.
[182] S. Hosseinpour, M. Aghbashlo, M. Tabatabaei, E. Khalife, Energy Convers. Manage. 124 (2016) 389–398.
[183] D. Kang, Y. Zhang, D.-G. Yu, I. Kim, W. Song, J. Nanobiotechnol. 23 (2025) 101.
[184] L. Zeng, D. Kang, L. Zhu, D.G. Yu, W. Song, Adv. Healthc. Mater. 14 (2025) 2404333.
[185] D. Kang, Y. Wen, Z. Wang, et al., Innov. Mater. 3 (2025) 100107.
[186] D. Kang, Y. Li, X. Dai, et al., Molecules 29 (2024) 5461.
[187] P.N. Bernal, S. Florczak, S. Inacker, et al., Nat. Rev. Mater. 10 (2025) 826–841.
[188] Y. Zhang, W. Song, S. Mao, et al., Small 21 (2025) 2408767.